Scientia Iranica A (2014) 21(4), 1249–1262

SCIENTIA IRANICA

Sharif University of Technology
Scientia Iranica
Transactions A: Civil Engineering
www.scientiairanica.com

Nonlinear finite element analysis of RC beams under combined shear and torsion to extract linear and curvilinear ranges of interaction curves

S.B. Talaeitaba[a,*] and M.E. Torki[b]

a. *PhD Graduate and Assistant Professor of Azad University, Department of Civil Engineering, Isfahan University of Technology, P.O. Box 8415683111, Isfahan, Iran.*
b. *PhD Student, Department of Aerospace Engineering, Texas A&M University, College Station, TX 77843, USA.*

Received 2 December 2012; received in revised form 4 September 2013; accepted 4 January 2014

KEYWORDS
Shear-torsion interaction curve; FEM analysis; Transverse reinforcement; Torque-twist curve.

Abstract. The use of non-linear finite elements to assess the effect of transverse reinforcement amount on the shape of shear-torsion interaction curve for RC beams is addressed. At first, FEM results for specimens under pure torsion and combined shear and torsion were validated with previous outcomes. Secondly, reference specimens were made with the minimum required transverse reinforcement at first. Each specimen was analyzed with the finite element method and tested under similar conditions in the laboratory, and the results, including the cracking pattern, cracking and ultimate loads, and shear-torsion interaction curves, were found to be in very good agreement. Finally, the transverse reinforcement amount was increased to certain extents and similar results were determined. FEM interaction curve stood below the experimental curve. It was also deduced that, from a certain increase in the transverse reinforcement, the shear-torsion interaction curve transforms from linear to elliptical.

1. Introduction

Dealing with the combined effects of shear and torsion dates back to about 70 years ago [1,2]. By using the skew bending method, shear-torsion interaction curves for RC beams were firstly put forward as circular or bilinear curves, depending on the ratio between flexure, shear, and torsion [3,4]. From a set of experimental data, it has been gathered that not only increasing the transverse reinforcement, but also reducing the concrete cover on the transverse bars and increasing the torsion-to-shear ratio (leading to shatter in the concrete cover), the shear-torsion interaction deviates from linear into curvilinear. This curve tends towards the vertical axis (pure torsion) perpendicularly [1,5]. A large cache of work exists in the literature regarding the issue of torsion in concrete beams, either alone or in a combined state with other loading schemes, which are truly concurrent with the results later expressed in the present research.

The torsional behavior of concrete elements was developed by Karayannis [6,7], expressed in terms of normal stress and crack width, for the behavior of concrete elements in increasing torsion, also applicable to concrete elements subjected to torsion combined with flexure, shear, and axial force. They deduced that increasing the transverse reinforcement does not bear a significant effect upon the cracking load. Moreover, assuming a simplified bilinear stress-strain curve for concrete, Karayannis and Chalioris [8]

*. *Corresponding author. Tel.: +98 311 3912701; Fax: +98 311 3912700*
E-mail addresses: talaeitaba@yahoo.com (S.B. Talaeitaba); mtorki@neo.tamu.edu and mtorki85@gmail.com (M.E. Torki)

used two-dimensional elements for the solution of a modified Poisson's equation within the Saint-Venant torsion theory for concrete beams without reinforcement. They presented material failure criteria considering the influence of prestressing forces in addition to torsional torque. A combination of two different theoretical models was adopted for concrete beams by Chalioris [9,10] in which the elastic response until initial cracking was described by the modified approaches of the classical elastic theory, and the post-cracking part was considered by specially extended versions of the softened truss model. These combined methods have been reported to provide full analytical torsional curves for the behavior of rectangular fibrous beams with conventional reinforcement outlines. Their results included a non-linear analysis for torsional concrete beams that yields to a realistic modeling of the entire (i.e. elastic and post-cracking) response of beams.

Chaisomphob and Kritsanawonghong [11] tested RC beams under combined double-axis shear and torsion. They set forth that the double-axis shear capacity becomes rigorously decreased when torsion exists. A nonlinear finite element method for analyzing the load-deflection behavior and failure characteristics of deep reinforced concrete coupling beams was developed by Zhao et al. [12]. Their investigation revealed that although adding more shear reinforcement can suppress shear-tension failure, it will cause shear-sliding failure at the beam-wall joints. Garcia and Bernat derived the interactive equations of beams under combined shear and torsion, solved them numerically, and verified their results with those obtained from nonlinear modeling [13]. Green and Belarbi plotted force-displacement curves for RC beam cross sections under shear, torsion, and bending by solving equations of equilibrium and consistency [14]. They validated their results with 28 experimental outcomes. Based on the Modified Compression Field Theory with a tangent-stiffness formulation and the Timoshenko beam theory, a model for the analysis of reinforced and prestressed concrete frame elements under combined loading axial, biaxial bending, torsion, and biaxial shear loadings was presented by Gregori et al [15]. They validated their results with well-known tests. Using a specifically-designed test setup subjecting the beam to combined shear and torsion with different ratios, the strengthening effects of FRP strips were investigated by Deifalla and Ghobarah [16] with four strengthening outlines for concrete T-shaped beams under combined shear and torsion. The extended U-jacket technique proved to show the most promising results in terms of strength and ductility while being quite feasible for strengthening. Seismic performance of concrete circular columns under cyclic bending and shear, cyclic pure torsion, and various levels of combined cyclic bending, shear, and torsion were presented by Prakash et al. [17]. They demonstrated that there is no considerable variation in flexural or torsional capacities with decrease in aspect ratio. However, their results showed a significant change in the failure mode and deformation characteristics due to reduction in aspect ratio. Based on the softened membrane model with a tangent-stiffness formulation and the Timoshenko beam theory, a three-dimensional (3D) concrete constitutive model for fiber-based analysis of concrete members subjected to combined loadings including torsion was implemented by Mullapudi and Ayoub [18] in order to evaluate the interactive behavior between the axial force, bidirectional shear, biaxial bending, and torsion. They emphasized the use of the model for the evaluation of the effect of the different stress states on the global and local behavior of concrete members.

The finite element modeling of RC structures subjected to shear deformations includes considerable work in the literature, but it demands more profound results with respect to the derivation of shear-torsion interaction curves emphasizing a complete range of transverse reinforcement amount. The present research aims at using nonlinear finite element analysis to evaluate the effect of transverse reinforcement amount on the shape of the shear-torsion interaction curve in RC beams. At first, the specimens are analyzed and tested with the minimum transverse reinforcement, required according to ACI 318, and the shear-torsion interaction curve is plotted. The FEM interaction curve, being slightly lower, is satisfying compared to that obtained from the experiment. Then, the transverse reinforcement is multiplied by different ratios, and the new interaction curve in each case is plotted to figure out in which ranges the interaction curve is linear, and in which ranges it is curvilinear.

2. Materials and method

2.1. Concrete

From the library of elements, SOLID65 (as a 3D element with 3 degrees of freedom at each node) was used for reinforced concrete. This class of elements allows the opportunity to define the reinforcement volumetric ratio (as the ratio of reinforcement volume to the element volume) in three orthogonal directions. The method used in the present research is nonlinear finite element which lies on the five-parameter William-Warnke yield model for concrete, defined as [19]:

$$\frac{F}{f_c} - S \geq 0, \tag{1}$$

where F is a function of principal stresses, S is the yield surface, and f_c is the concrete uniaxial crushing stress. The parameters of influence in this model are the concrete elasticity modulus (E_c), the maximum

uniaxial compressive stress in concrete (f'_c), the maximum tensile stress in concrete, i.e. rupture modulus (f_r), Poisson's ratio (ν), the shear transfer coefficients in open and closed cracks (β_t and β_c, respectively), and the uniaxial compressive stress-strain curve for concrete. Among all parameters, the second and third parameters bear the utmost influence on the yield surface. Generally, a concrete element cracks whenever the principal tensile stress lies out of the yield surface. On the other hand, an element is said to crush when all the three principal stresses are compressive and lie out of the yield surface. In the former case, the elasticity modulus becomes zero along the direction normal to the cracking principal stress, and in the latter case, it is considered to be zero along all principal directions, implicating that the element is computationally omitted [20]. The schematic shape of this yield surface is shown in Figure 1 [20].

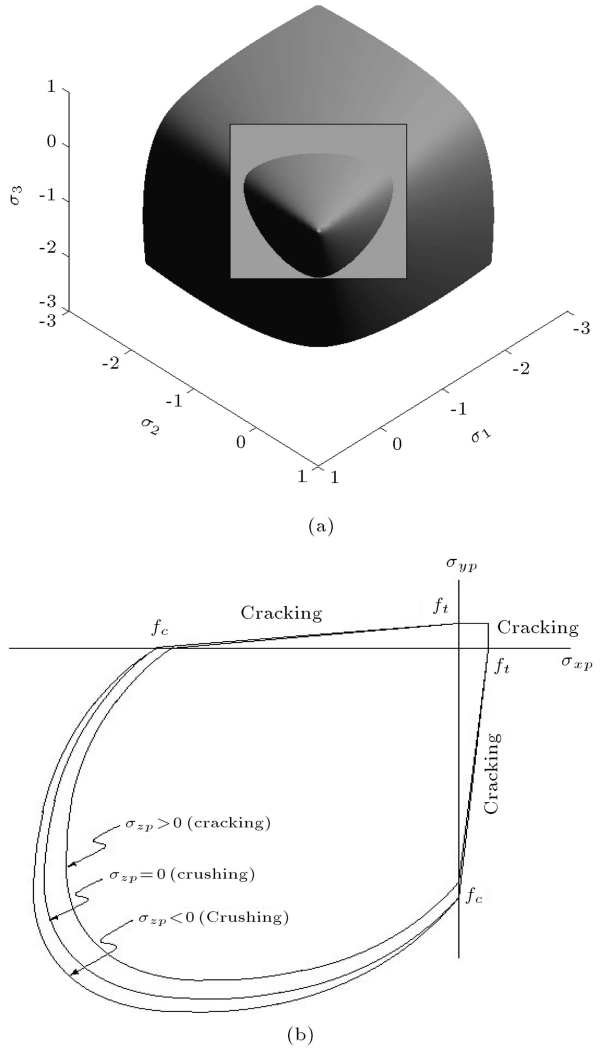

Figure 1. William-Warnke computational yield surface: (a) An example of the general 3D surface (en.wikipedia.org/wiki/Willam-Warnke_yield_criterion); and (b) the biaxial sub-surface.

The elasticity and rupture moduli of concrete in this research were obtained, respectively, using the expressions (in MPa).

$$E_c = 5000\sqrt{f'_c}, \tag{2}$$

$$f_r = 0.67\sqrt{f'_c}. \tag{3}$$

Furthermore, the Poisson's ratio was considered to be 0.2. The values of β_t were different in prismatic specimens (made for verification of calculations with previous results), and non-prismatic ones (main specimens used in the present investigation), which will be pointed out in the corresponding sections. The value of β_c has been suggested to be taken unity all the time. However, numerous analyses have proven that for better convergence, β_c is better to be considered slightly smaller than unity, e.g. 0.99, the value considered in all calculations in the present research [20-23]. An important fact in concrete fracture is that in most practical cases, pure compressive fracture is improbable [23]. Even in a uniaxial compressive test, secondary tensile stresses (induced due to the Poisson effect) bring about cracking and yielding. Therefore, to have a realistic model, the crushing ability of concrete has to be prevented [19]. This can be done by taking f'_c to be -1 [20]. After initial cracking, the tensile strength of the cracked cross section is reduced as multiplied by a reduction factor T_c, which is mostly considered to be 0.6. After initial cracking, the mechanical behavior of concrete depends on a reduced secant modulus named R_t, as shown in Figure 2. The concrete's post-cracking elasticity matrix is modified according to this parameter, as included in Appendix A.

2.2. Reinforcement

It may be specious to use a prescribed reinforced solid element, which defines the reinforcement as the volumetric ratio of reinforcement to concrete. However, this has not proven to be the best way because the exact location of the bar is unknown, and even worse, full adhesion is considered between concrete and the bars, which is not a realistic assumption. Instead, it

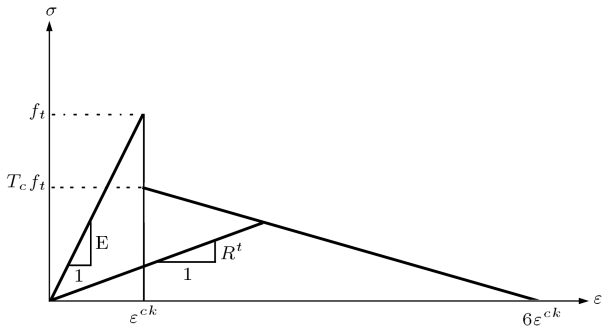

Figure 2. Tensile stress deterioration after initial cracking.

Table 1. Properties of specimens under pure torsion.

Specimen's code	Length (mm)	Shape and dimensions of the cross section	Transverse reinforcement amount	Longitudinal reinforcement amount	f'_c (MPa)
N1	2440	Rec.150 * 350 mm	ϕ6.32@120 mm $f_y = 456.8$ MPa	top: 2ϕ11.3 mm $f_y = 400$	37.0
N2			ϕ6.32@70 mm $f_y = 456.8$ Mpa	bot: 2ϕ16 $f_y = 409$ Mpa	
N3			ϕ6.32@200 mm $f_y = 567$ Mpa	top: 2ϕ11.3 mm $f_y = 400$ bot: 2ϕ19.4 $f_y = 461$ Mpa	
RC	1900	Rec.150*350 mm	ϕ6@80 mm $f_y = 251$ Mpa	4ϕ16 mm in corners $f_y = 502$ Mpa	39.0
RG					36.0
Rb-s5.5/160	1000	Rec.150*300 mm	ϕ5.5@160 mm $f_y = 350$ Mpa	4ϕ8 mm in corners $f_y = 560$ Mpa	28.8
Ref	3960	Rec.279.4*279.4 mm	ϕ9.53 mm@152.4 $f_y = 420$ Mpa	Corner: 4ϕ12.7 $f_y = 460$ Mpa Sides: 4ϕ9.53	34

Table 2. Comparison between FEM and experimental results in specimens under pure torsion.

Specimen's code	Cracking load from experiment (kN)	Ultimate load from experiment (kN)	Cracking load from FEM (kN)	Ultimate load from FEM (kN)
N1	5.32	12.88	5.22	12.10
N2	5.88	12.80	5.93	11.81
N3	6.59	12.59	6.40	12.01
RC	9.50	15.00	7.65	11.80
RG	8.00	14.80	6.72	13.09
Rb-s5.5/160	6.92	—	5.69	7.21
Ref.	17.00	18.00	13.60	19.42

is expedient to model the bars separately by using link elements, for which LINK 8 was picked from the library, which is a 3D truss element with 3 degrees of freedom at each node. This method is in all aspects preferable to the other reported method [20], since it especially helps to model more conveniently, enables to define the reinforcement in every direction without changing the whole element direction, and the analysis will be more time-efficient. Hence, this method has been recommended by the software manual. The von Mises yield criterion was used for the steel reinforcement bars with a tri-linear stress-strain behavior. The analyses include the validation of models with those of the existing literature and the new innovative results of the present research as comes in the sequel.

3. Verification and comparison

3.1. Specimens under pure torsion

In the first step, cantilevered specimens undergoing pure torsion were adopted from previous works. The geometric and reinforcement parameters of these specimens are included in Table 1. Figure 3 shows the finite element model of one of these models.

As many references have recommended (for prismatic models), β_t was taken to be 0.4 for better convergence of analysis [19-22]. To forestall the analysis divergence due to stress concentration under the loaded points, the elements in a length equaling the cross section height from the loaded points were considered devoid of any cracking and nonlinear behavior. The loading scheme was load-controlled analysis. Table 2 includes the comparison between FEM and experimental results for cracking and ultimate loads.

Moreover, the cracking patterns in FEM and experimental models are identical, as shown in Figures 4 and 5.

Finally, the torque-twist curves, as shown in Figure 6 for N2 specimen, are consistent up to the cracking threshold. However, after cracking initiation, the FEM curve does not have enough precision. This lies in the fact that the open-crack shear transfer

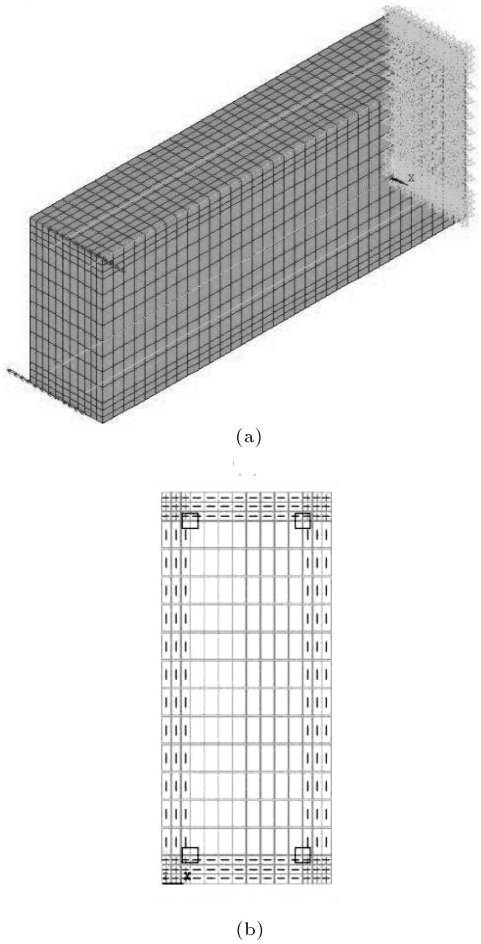

Figure 3. Meshing and modeling of a specimen under pure torsion.

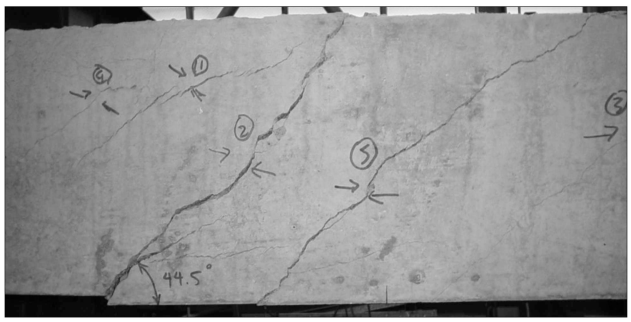

Figure 4. Cracking pattern in the experimental specimen.

coefficient after cracking initiation is a small value. This makes the corresponding element of the stiffness matrix (according to Appendix A) too small, and thus the analysis loses exactitude. However, the FEM analysis gives the ultimate (fracture threshold) load truly [24].

3.2. Specimens under combined shear and torsion

In the second stage, FEM analyses were compared to those obtained from Rahal's experiments [1]. The

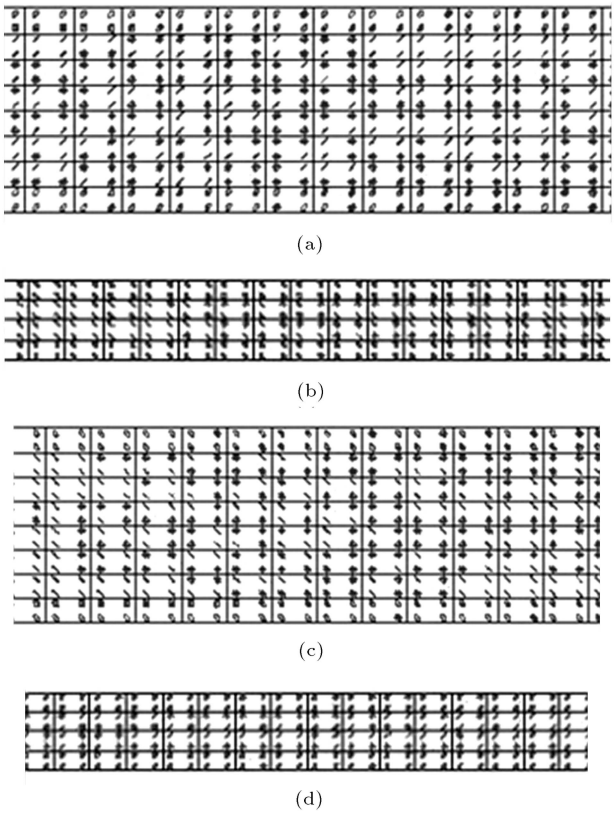

Figure 5. Cracking pattern in the FEM model: (a) Left face; (b) up face; (c) right face; and (d) down face.

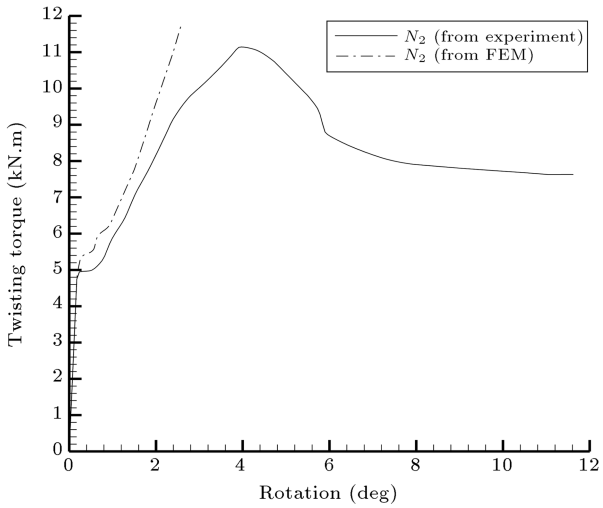

Figure 6. Torque-twist curve belonging to N_2.

geometric and reinforcement parameters of this model are shown in Figure 7. Each specimen was made with this model and a specific load eccentricity (i.e. the torsion to shear ratio). The reinforcement bars had a bilinear stress-strain curve, in which the post-yielding modulus was 5 percent of the initial (elasticity) modulus. The longitudinal bars had 25 mm diameters, the yield stress of 480 MPa, and the ultimate stress of 466 MPa. All the same, the transverse bars had 10 mm

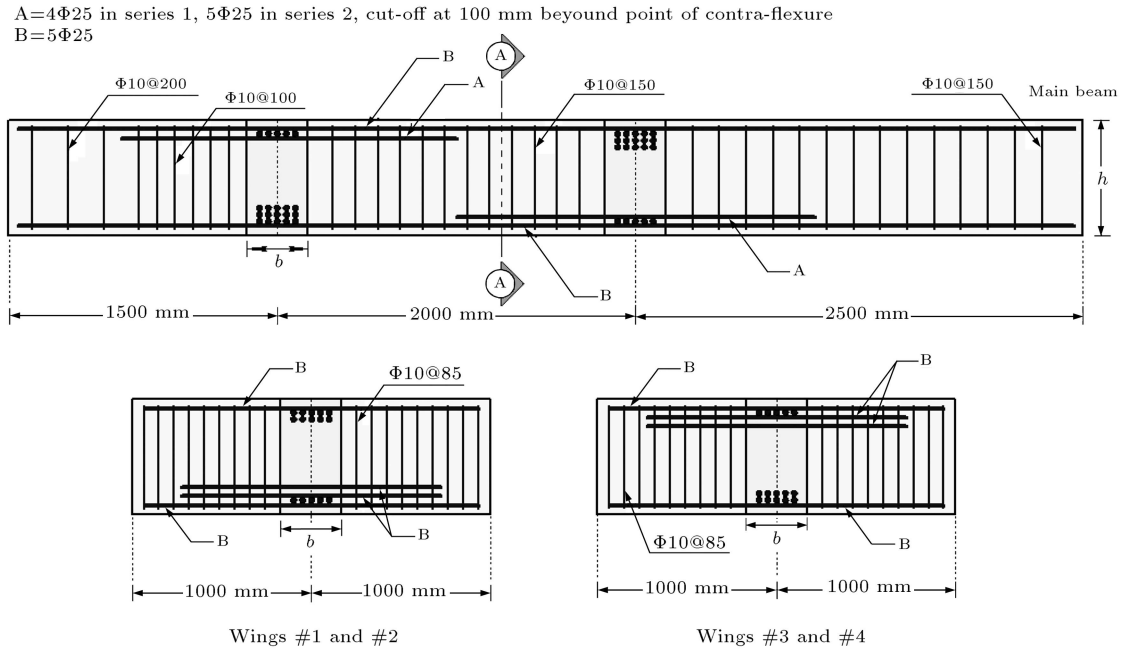

Figure 7. Geometric and reinforcement properties of Rahal's models.

Table 3. Mechanical properties of Rahal's models.

Specimen no.	Specimen's code	Eccentricity (mm)	Compressive strength (MPa)	Ultimate strain ($\times 10^{-3}$)	Concrete elasticity modulus (MPa)
1	RC2-1	162	53.9	2.25	39400
2	RC2-2	0	38.2	2.80	28300
3	RC2-3	1500	42.2	2.25	38530
4	RC2-4	80	48.7	2.21	31500

diameters, the yield stress of 676 MPa, and the ultimate stress of 626 MPa. The models were made in the same way as the purely torsional models had been made. The proposed specimens in this reference are included in Table 3. The cracking pattern was identical in both experimental and FEM results. For instance, the RC2-2 cracked specimen in the laboratory and the cracked FEM model are shown in Figure 8. Moreover, the cracking and ultimate loads, obtained from experiment and FEM analysis, for different specimens, are included in Table 4. It can be observed that the results are quite coincident. On the other hand, as for the case of purely torsional models, after initial cracking, the torque-twist curve obtained from FEM analysis is not in full agreement with that obtained from experiment, as shown in Figure 9 for RC2-4. The reason is the same as that stipulated for the purely torsional models.

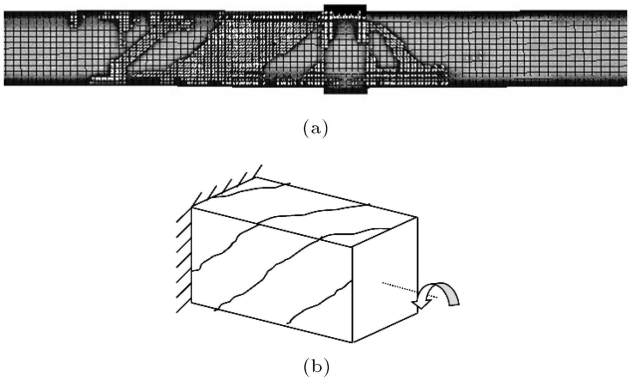

Figure 8. Cracking outline in the FEM analyzed RC2-2 specimen.

4. Modeling the main specimens

4.1. Geometric and reinforcement properties

The modeling procedure of the main specimens of the present research is being addressed in this section. The support conditions were clamped-clamped because of the special characteristics of the loading apparatus [25]. The ends were clamped against bending and torsion, and the eccentric load was applied at the middle (and the centric load was applied as pure shear). Because of the restrictions in the experimental test apparatus, it was inconvenient, however possible, to make a multi-bay beam. Instead, the non-prismatic assemblage

shown in Figure 10 was prepared. This lies upon the fact that, on the basis of the designed supporting system, the zone with negligible bending moment stands in the two end quarters of the length in the proximity of contraflexure points, i.e. in the reduced cross section zones. The beam cross section and its transverse reinforcement (hoops) were reduced in these zones to concentrate the shear-torsion fracture zone to these regions. Otherwise, the ultimate load, and thus the moment in the middle and the ends would have increased, and this would have intertwined the flexural and shear-torsional behaviors in fracture. However, the beam ends had to have larger cross sections to provide sufficient rigidity at the clamped supports.

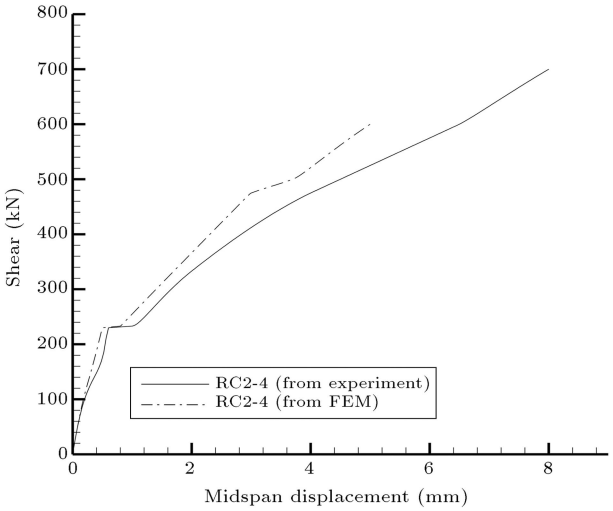

Figure 9. The shear-displacement curve belonging to RC2-4 specimen.

On the other hand, the longitudinal and transverse (hoop) reinforcements were increased in zones with high bending moments (to prevent flexural or, less probably, shear-torsional fracture from happening in those regions) and decreased to the minimum requirement stated in ACI 318-08 [26] in the reduced cross sections (to reassure that shear-torsional fracture occurs in these cross sections). Moreover, the longitudinal and transverse reinforcing bars in the flexural zone were made of steel with a 400 MPa tensile strength and had 16 and 8 mm diameters, respectively. However, the hoops used in the reduced sections (i.e. the test regions) had 4 mm diameter and had 240 MPa tensile strength. The concrete used in all specimens had a 35 MPa compressive strength. Table 5

Table 4. Cracking and ultimate loads for Rahal's specimens.

Specimen's code	Cracking shear from experiment (kN)	Ultimate shear from experiment (kN)	Cracking shear from FEM (kN)	Ultimate shear from FEM (kN)
RC2-1	137	533	133	464
RC2-2	240	796	230	776
RC2-3	64	111	64	94
RC2-4	233	715	228	715

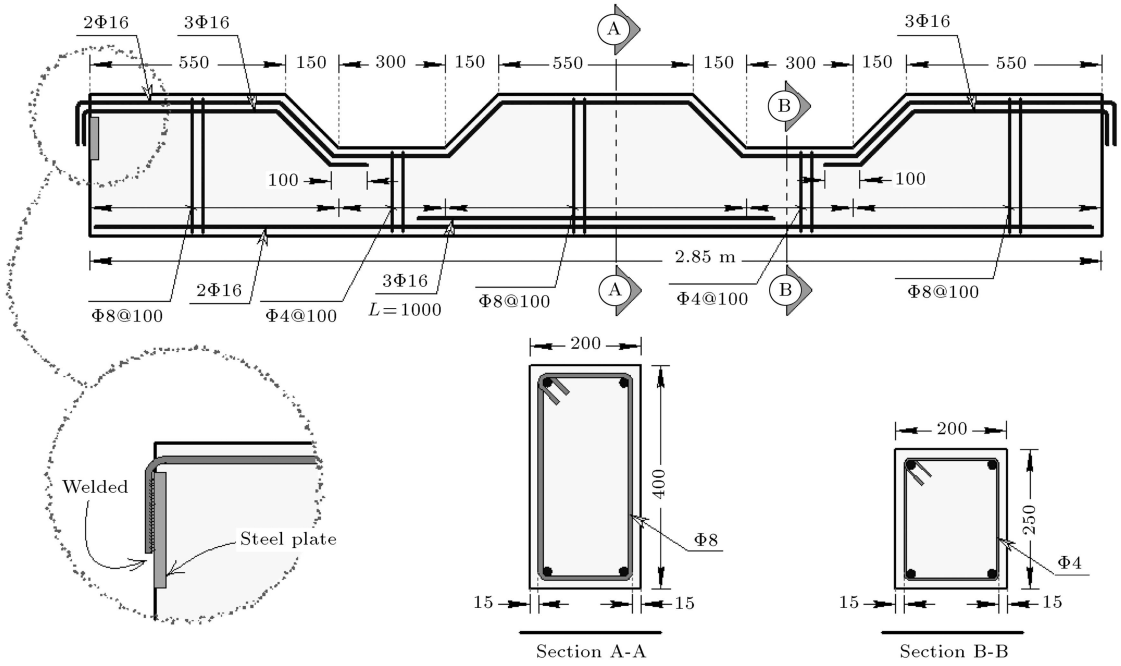

Figure 10. Specimens dimension and reinforcement (all dimensions in mm).

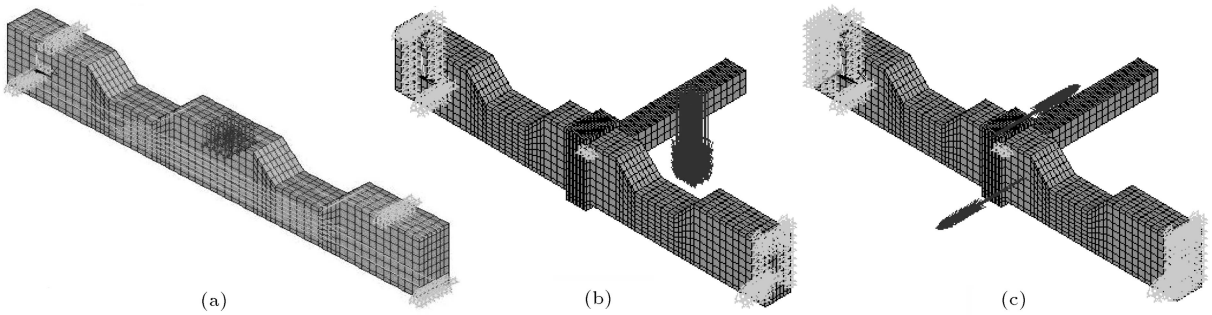

Figure 11. The finite element model of a main specimen: (a) Under pure shear; (b) under combined shear and torsion; and (c) under pure torsion.

Table 5. Main specimens' properties.

Specimen's code	Eccentricity (mm)
E0	0
E1	290
E2	470
E3	616
E4	∞

includes the specimens' names and each specimen's load eccentricity, ranging from zero (pure shear) to infinity (pure torsion). The twisting rotation was measured by using two LVDTs on the middle cross section width ends, and dividing the difference of the measured digits by the cross section width. Due to the structural weakness induced by reducing the section at the proximity of the contraflexure points, fracture occurred in the reduced zone in all specimens, and the bigger section had only rigid movement. Hence, the twisting torque-vs.-twisting rotation curves for all specimens depend directly on the behavior of the reduced section.

4.2. Finite element model

As stated in the above, concrete was modeled using solid elements. The elements without transverse reinforcement were considered to be devoid of volumetric reinforcement, and those including transverse reinforcement were identified by specifying the bar-to-element volumetric ratio along the direction of the transverse bars (hoops). However, the longitudinal bars were modeled separately by using link elements along the longitudinal direction. Figure 11 shows the meshing and reinforcing of the model used in the present research. The metal belt around the beam was modeled using solid elements made of steel, with full adhesion to the concrete elements. After numerous analyses, the optimum values of β_t and β_c were obtained to be 0.05-0.25 (depending on the model, but can be considered the average value of 0.2 in most cases) and 0.99, respectively [19]. The minimum transverse reinforcement was firstly used in specimens and each specimen was analyzed under different shear load eccentricities (with the eccentricity defined as the torsion to shear ratio) and FEM results were compared to those obtained from experiment. Secondly, the transverse reinforcement amount was increased according to Subsection 5.5 and new FEM models were made and analyzed likewise.

5. Results and discussion

5.1. Cracking pattern

Figure 12 shows the cracking pattern belonging to one of the specimens, which is in complete agreement with the spiral cracking pattern observed in the laboratory. The small dashes and the complete squares show the cracked and inept paths, respectively.

5.2. Cracking and ultimate loads

The cracking and ultimate loads for all specimens are included in Table 6. It can be realized that there is satisfactory agreement between the results.

5.3. Curves of behavior

The torque-twist curves for different specimens are shown in Figure 13 as compared to the experimental curves. It can be observed that the initial behaviors of the two curves are in complete match. However, as seen in all cases in Section 4, the FEM curve stops after initial cracking for the same reason as theorized in Section 4. It can be seen that, in all cases, the ultimate (capacity) load (either pure shear or twisting torque) value obtained from FEM analysis is smaller than that obtained from experiment.

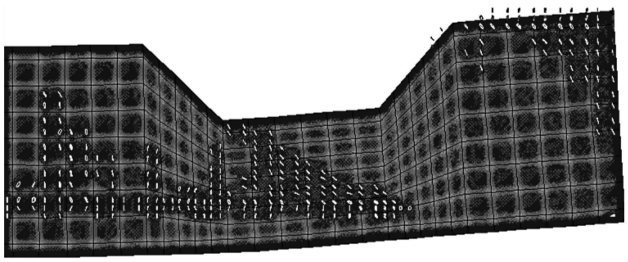

Figure 12. Cracking in a main specimen.

Table 6. Cracking and ultimate loads for main specimens.

Specimen's code	Cracking load from experiment (kN)	Ultimate load from experiment (kN)	Cracking load from FEM (kN)	Ultimate load from FEM (kN)
E0	100.0	134.0	103.1	127.0
E1	38.0	49.2	35.5	46.9
E2	21.0	33.7	20.8	32.0
E3	18.0	29.0	16.5	28.2
E4	20.0	55.0	19.8	50.2

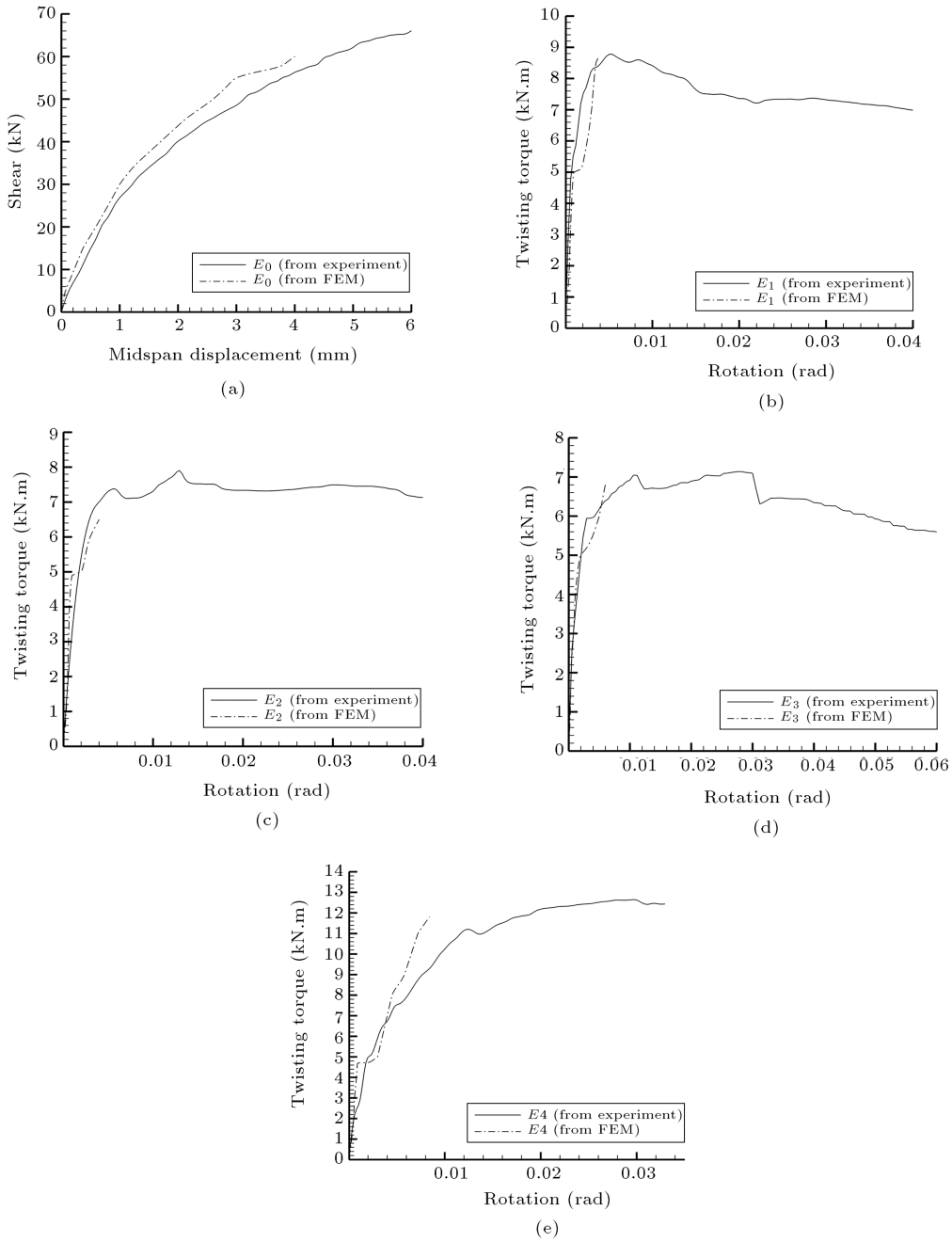

Figure 13. Torque-twist curves for main specimens.

5.4. Interaction curves

The ultimate (capacity) shear-torsion interaction curve, including the data of all 5 specimens, is shown in Figure 14. This figure reveals that, on the one hand, the interaction curve, either from FEM analysis or from experiment, can be considered linear although both curves deviate slightly downward in the 470 mm load eccentricity. On the other hand, since the ultimate load from FEM calculation is smaller than that determined by experiment, the FEM interaction curve stands below the experimental curve.

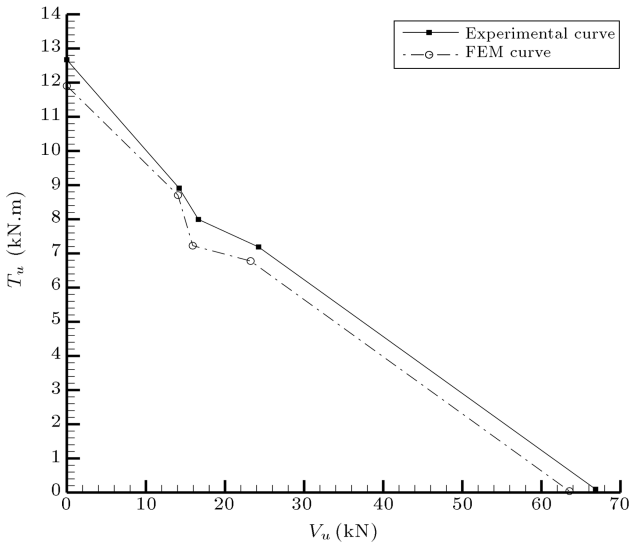

Figure 14. Shear torsion interaction curve for the minimum required transverse reinforcement.

5.5. Effect of transverse reinforcement on the interaction curve.

Considering the transverse reinforcement amount as the comparator, this section contains the effect of increasing the transverse reinforcement amount on the shape of the shear-torsion interaction curve. For this purpose, the reference transverse reinforcement amount in the reduced cross section (equaling the minimum requirement according to ACI 318-08 [26]) has been multiplied by 2, 3, 4 and 5. The new specimens' properties are included in Table 7. As an instance, the twisting rotation curves for E1-E15 specimens in a 290 mm load eccentricity are given in Figure 15.

In order to compare the effect of transverse reinforcement more appropriately, the cracking and ultimate loads for different transverse reinforcement amounts in the reduced cross section have been plotted against the ratio of the increased transverse reinforce-

Table 7. Specimens with increased transverse reinforcement amount.

No.	Specimen's code	Equivalent transverse reinforcement amount (mm)	Eccentricity (mm)	Ratio of the transverse reinforcement to the minimum requirement
1	E02	ϕ6@100	0	2
2	E12		290	
3	E22		470	
4	E32		616	
5	E42		∞	
6	E03	ϕ8@120	0	3
7	E13		290	
8	E23		470	
9	E33		616	
10	E43		∞	
11	E04	ϕ10@145	0	4
12	E14		290	
13	E24		470	
14	E34		616	
15	E44		∞	
16	E05	ϕ10@120	0	5
17	E15		290	
18	E25		470	
19	E35		616	
20	E45		∞	

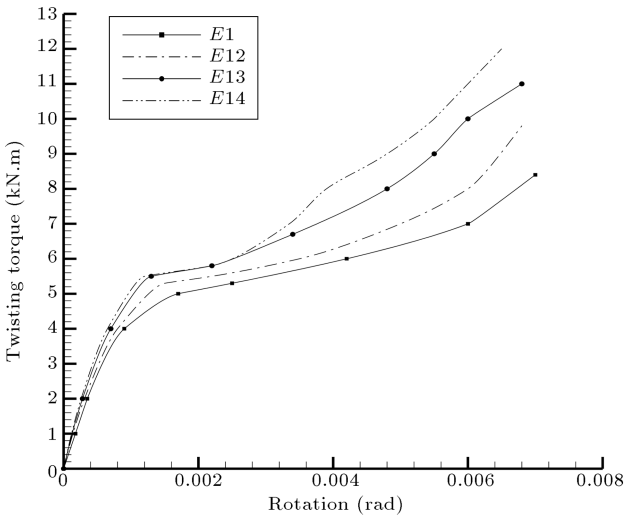

Figure 15. Torque-twist curves of main specimens in the 290 mm eccentricity.

ment to the reference reinforcement in Figure 16. This figure reveals the following results:

1. Increasing the transverse reinforcement amount does not have a significant effect on the cracking load, especially for specimens under combined shear and torsion (from E1 onwards). However, it considerably increases the ultimate load. Thus, the initial slope of the torque-twist curve remains almost unvaried while the ultimate slope becomes remarkably increased with the transverse reinforcement. The effect of increasing the transverse reinforcement is maximum, both in cracking and ultimate loads, for the specimen under pure shear (E0), and it decreases with the load eccentricity (in specimens under combined shear and torsion).
2. By increasing the transverse reinforcement amount, the ultimate load increases linearly up to the transverse reinforcement ratio of 3. For greater ratios, it increases by more than the corresponding linear increase. For this reason, the ultimate shear-torsion interaction curves remain linear up to the ratio of 3. However, for greater ratios, the curves become elliptical rather than linear. This phenomenon is in exact coincidence with previous research outcomes and the fact underlying this occurrence is the more brittle behavior of the structure happening due to concrete tearing off from the surface of the surface around the bars [1]. The interaction curves for different transverse reinforcement ratios are shown in Figure 17 (the numerical data are given in Appendix B).

6. Conclusions

The present research contains nonlinear finite element analysis of reinforced concrete beams under

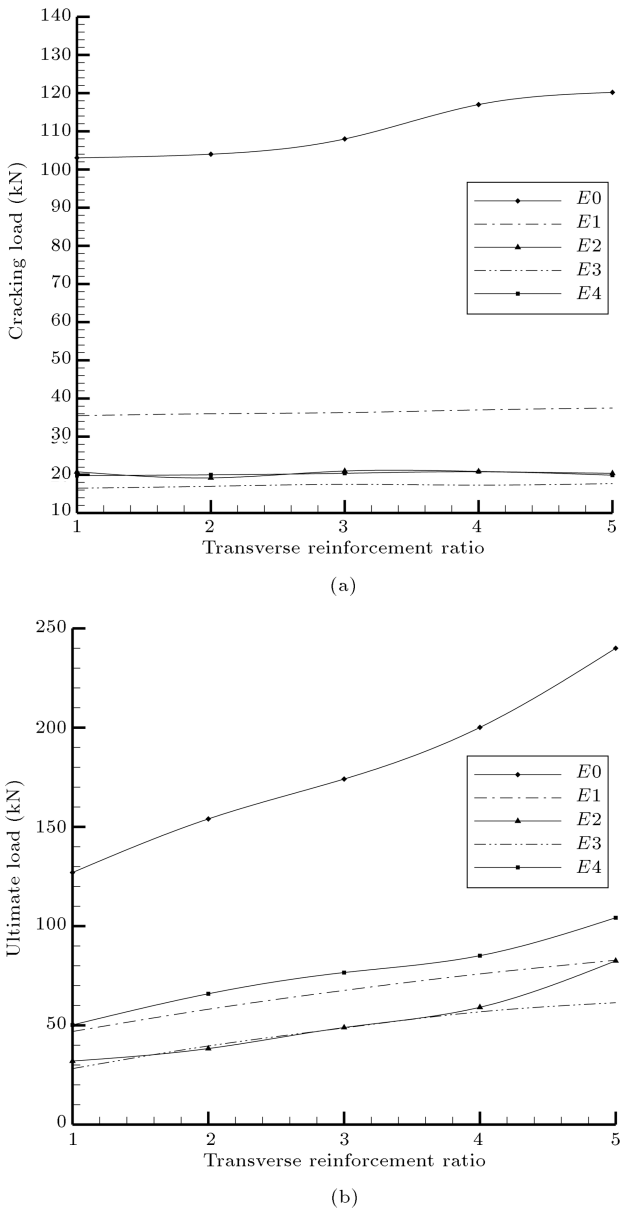

Figure 16. Effect of transverse reinforcement amount in the reduced cross section: (a) On the cracking load; and (b) on the ultimate load.

combined shear and torsion to evaluate the effect of transverse reinforcement amount on the shape of shear-torsion interaction curve. In this respect, FEM models were firstly made to verify the results with previous investigations for pure torsion and combined shear-torsion. Then, main models were made with a clamped-clamped boundary condition and a non-prismatic cross section along the longitudinal direction. Each model, with the transverse reinforcement equal to the minimum required amount and a specific load eccentricity, was analyzed with nonlinear finite element and the cracking pattern, cracking and ultimate loads were obtained and validated with experiment. The cracking paths as well as the cracking and ultimate

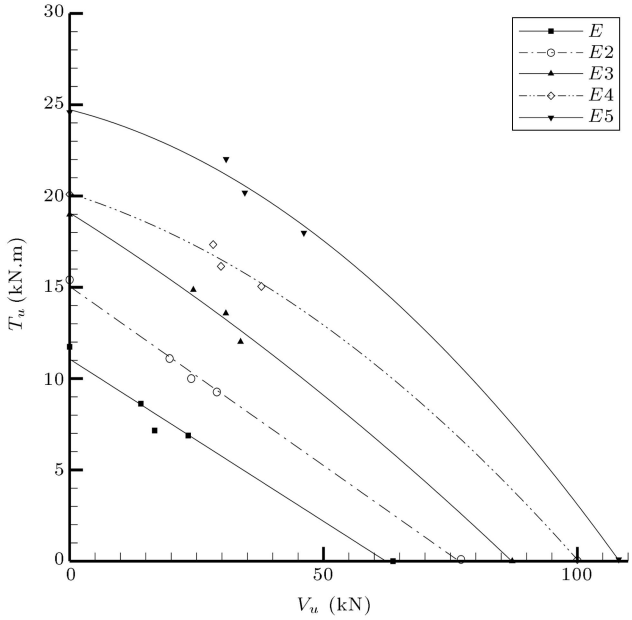

Figure 17. Shear-torsion interaction curves for different specimens (with different transverse reinforcement amounts).

loads were in complete accordance with experimental data, even though the post-cracking load-deflection curve obtained from FEM analysis was not realistically evaluated. Although FEM and experimental cracking and ultimate loads were found to be in satisfactory accordance, the interaction curve obtained from FEM stood below the experimental curve. Finally, shear-torsion interaction curves for specimens with higher transverse reinforcement amounts (defined as the ratio of the transverse reinforcement amount to the minimum ACI 318 requirement) were extracted with FEM analysis. It was seen that the curve remains linear up to the transverse reinforcement ratio of 3, and becomes elliptical for larger ratios. This happens due to the concrete tearing off from the surface around the reinforcement bars.

Nomenclature

E_c	Concrete elasticity modulus
f_r	Rupture modulus (maximum tensile stress in concrete)
F	A function of principal stresses in the yield model
F_c	Concrete uniaxial crushing stress
f'_c	Maximum uniaxial compressive stress of concrete
R_t	Reduced secant modulus in the post-cracking stiffness matrix
S	Yield surface function
T_c	Tensile strength reduction factor after initial cracking
β_t	Shear transfer coefficient in open cracks
β_c	Shear transfer coefficient in closed cracks
ν	Poisson's ratio

References

1. Rahal, K.N., "The behavior of reinforced concrete beams subjected to combined shear and torsion", PhD Thesis, University of Toronto (1993).

2. Mc Mullen, E. and Warwaruk, J. "Concrete beams in bending, torsion and shear", *Proceeding of the American Society of Civil Engineering, Journal of the Structural Division*, **96**, pp. 885-903 (1970).

3. Hsu, T.C. "Ultimate torque of reinforced rectangular beams", *Proceeding of the American Society of Civil Engineering, Journal of the Structural Division*, **94**, pp. 485-511 (1968).

4. Klus, J.P. "Concrete beams under combined torsion and shear", *ACI Journal*, pp. 210-216 (1968).

5. Hsu, T.C. "Unified theory of reinforced concrete", *CRC Press, Inc.*, Boca Raton, Fla (1993).

6. Karayannis, C.G. "Smeared crack analysis for plain concrete in torsion", *Journal of Structural Engineering ASCE*, **126**(6), pp. 638-645 (2000).

7. Karayannis, C.G. and Chalioris, C.E. "Experimental validation of smeared analysis for plain concrete in torsion", *Journal of Structural Engineering ASCE*, **126**(6), 646-653 (2000).

8. Karayannis, C.G. and Chalioris, C.E. "Strength of prestressed concrete beams in torsion", *Journal of Structural Engineering and Mechanics*, **10**(2), pp. 165-180 (2000).

9. Chalioris, C.E. "Experimental study of the torsion of reinforced concrete members", *Journal of Structural Engineering and Mechanics*, **23**(6), pp. 713-737 (2006).

10. Chalioris, C.E. "Analytical model for the torsional behaviour of reinforced concrete beams retrofitted with FRP materials", *Journal of Engineering Structures*, **29**(12), pp. 3263-3276 (2007).

11. Chaisomphob, T., Kritsanawonghong, S. and Hansapinyo, C. "Experimental investigation on rectangular reinforced concrete beam subjected to bi-axial shear and torsion", *Songklanakarin Journal of Science and Technology*, **25**(1), pp. 41-52 (2003).

12. Zhao, Z.Z., Kwan, A.K.H. and He, X.G. "Nonlinear finite element analysis of deep reinforced concrete coupling beams", *Journal of Engineering Structures*, **26**(1), pp. 13-25 (2004).

13. Garcia, J.M.B. and Bernat, A.R.M. "Shear-bending-torsion interaction in structural concrete members: A nonlinear coupled sectional approach", *Journal of Architecture Computational Methods in Engineering*, **14**, pp. 249-278 (2007).

14. Green, G. and Belarbi, A. "Model for reinforced concrete members under torsion, bending, and shear. I: Theory", *Journal of Engineering Mechanics, ASCE*, **135**(9), pp. 961-969 (2009).

15. Gregori, J.N., Sosa, P.M., Prada, M.A. and Filippou, F.C. "A 3D numerical model for reinforced and prestressed concrete elements subjected to combined axial, bending, shear, and torsion loading", *Journal of Engineering Structures*, **29**, pp. 3404-3419 (2007).

16. Deifalla, A. and Ghobarah, A. "Strengthening RC T-beams subjected to combined torsion and shear using FRP fabrics: Experimental study", *Journal of Composites for Construction, ASCE*, **14**, pp. 301-311 (2010).

17. Prakash, S., Belarbi, A. and You, Y.M. "Seismic performance of circular RC columns subjected to axial force, bending, and torsion with low and moderate shear", *Journal of Engineering Structures*, **32**, pp. 46-59 (2010).

18. Mullapudi, T.R.S. and Ayoub, A. "Analysis of reinforced concrete columns subjected to combined axial, flexure, shear, and torsional loads", *Journal of Structural Engineering, ASCE*, **139**, pp. 561-573 (2013).

19. Willam, K.J. and Warnke, E.P. "Constitutive models for the triaxial behavior of concrete", *Proceedings of the International Assoc. for Bridge and Structural Engineering*, **19**, pp. 1-30 (1975).

20. Mostofinejad, D. and Talaeitaba, S.B. "Nonlinear modeling of RC beams subjected to torsion using the smeared crack model", *Journal of Procedia Engineering*, **14**, pp. 1447-1454 (2011).

21. Hii, A.K.Y. and Al-Mahaidi, R. "An experimental and numerical investigation on torsional strengthening of solid and box-section RC beams using CFRP laminates", *Journal of Composite Structures*, **75**, pp. 213-221 (2006).

22. Kachlakev, D., Miller, T., Yim, S., Chansawat, K. and Potisuk, T. "Finite element modeling of reinforced concrete structures strengthened with FRP laminates", *Final Report SPR* 316 (2001).

23. Hemmaty, Y. "Modeling of the shear force transferred between cracks in reinforced and fiber reinforced concrete structures", *Proceedings of the ANSYS Conference*, Pittsburgh, Pennsylvania, USA, **1**, pp. 123-138 (1998).

24. Najim Mahmood, M. "Nonlinear analysis of reinforced concrete beams under pure torsion", *Journal of Applied Science*, **7**(22), pp. 3524-3529 (2007).

25. Talaeitaba S.B. and Mostofinejad, D. "A new test setup for experimental test of RC beams under combined shear and torsion", *Journal of Advanced Materials Research*, **335, 336**, pp. 355-358 (2011).

26. ACI 318-08: Building Code Requirement for Structural Concrete (ACI318M-02) and Commentary-ACI 318R-08, *American Concrete Institute*, Farming Hills, MI, USA (2008).

Appendix A

The concrete post-cracking elasticity matrix:

$$\mathbf{D'}_c = \frac{E}{(1+\nu)} \begin{bmatrix} \frac{R^t(1+\nu)}{E} & 0 & 0 & 0 & 0 & 0 \\ 0 & \frac{1}{1-\nu} & \frac{\nu}{1-\nu} & 0 & 0 & 0 \\ 0 & \frac{\nu}{1-\nu} & \frac{1}{1-\nu} & 0 & 0 & 0 \\ 0 & 0 & 0 & \frac{\beta_t}{2} & 0 & 0 \\ 0 & 0 & 0 & 0 & \frac{1}{2} & 0 \\ 0 & 0 & 0 & 0 & 0 & \frac{\beta_t}{2} \end{bmatrix}$$

Appendix B

Numerical data for Figure 17 is as follows:

E		E_2		E_3		E_4		E_5	
V_u (kN)	T_u (kN. m)	V_u	T_u	V_u	T_u	V_u	T_u	V_u	T_u
0.00	11.55	0.00	15.29	0.00	19.14	0.00	20.06	0.00	24.66
14.07	8.63	19.65	11.04	24.28	14.73	28.33	17.08	30.85	21.80
17.32	7.31	24.06	9.90	30.61	13.41	30.05	16.22	34.88	20.25
23.66	6.91	29.24	9.21	34.06	12.26	38.11	15.13	46.57	18.13
62.58	0.00	77.17	0.00	87.35	0.00	100.02	0.00	108.27	0.00

Biographies

Sayed Behzad Talaeitaba is a PhD graduate of civil engineering from Isfahan University of Technology and an assistant professor of Azad University. His professional background includes the coordination of the structural design team at Faratarh Ariana Corporation, and his research interests include the mechanical properties of FRP reinforced concrete.

Mohammad Ebrahim Torki is a PhD research assistant at the Department of Aerospace Engineering, Texas A&M University, College Station, TX. He has been a lecturer at Azad University, and his research interests include mechanics of composite materials and fracture mechanics.